

Article

Preparation and Optimization of Steel Slag-Desulfurization Gypsum Composites Based on Interception of Arsenic-Contaminated Water at the Ground Surface

Yunyun Li ¹ , Yubo Sun ¹, Wentao Hu ^{1,*}, Dongfang Wang ^{1,2,*}, Dongxu Wu ¹, Wen Ni ¹ and Shanshan Yang ¹

¹ Key Laboratory of High-Efficient Mining and Safety of Metal Mines, Ministry of Education (USTB), University of Science and Technology Beijing, Beijing 100083, China; lyyustb@163.com (Y.L.); m202310110@xs.ustb.edu.cn (Y.S.); u202140060@xs.ustb.edu.cn (D.W.); niwen@ces.ustb.edu.cn (W.N.); shanshan@163.com (S.Y.)

² BGRIMM Technology Group, Beijing 100160, China

Abstract: Based on the characteristics and effective components of steel slag and desulfurization gypsum, a new type of permeable reactive material was prepared by combining steel slag and desulfurization gypsum, and a simulation experiment of arsenic- and antimony-contaminated groundwater remediation was carried out. A combination of X-ray fluorescent, BGRIMM Process Mineralogy Analyzing System (BPMA), ICP-MS, and SEM-EDS detection and analysis methods was used to investigate the effects of steel slag particle size, desulfurization gypsum particle size, steel slag and desulfurization gypsum ratio, and steel slag-desulfurization gypsum mixed test block particle size on the performance of the permeable reactive wall to remove arsenic and antimony. The results show that a permeable reactive wall composed of steel slag ($-4.75 + 1.18$ mm) and desulfurization gypsum ($-13.2 + 9.5$ mm) in a 4:1 ratio achieved removal rates of 91.85% for As and 90.58% for Sb, reducing their concentrations below the drinking water standard. The purpose of using steel slag and desulfurization gypsum to intercept heavy metals and toxic ions in surface runoff was achieved. Arsenic was adsorbed, physically encapsulated, and lattice solidified by C-S-H gel. This research provides a cost-effective and environmentally friendly solution for the storage of steel slag and desulfurization gypsum while addressing heavy metal pollution in groundwater.

Keywords: steel slag; desulfurization gypsum; permeable reactive barrier; groundwater pollution; heavy metals; arsenic; intercepting material



Academic Editor: Meiry Gláucia Freire Rodrigues

Received: 8 February 2025

Revised: 14 March 2025

Accepted: 26 March 2025

Published: 31 March 2025

Citation: Li, Y.; Sun, Y.; Hu, W.; Wang, D.; Wu, D.; Ni, W.; Yang, S. Preparation and Optimization of Steel Slag-Desulfurization Gypsum Composites Based on Interception of Arsenic-Contaminated Water at the Ground Surface. *Processes* **2025**, *13*, 1033. <https://doi.org/10.3390/pr13041033>

Copyright: © 2025 by the author. Licensee MDPI, Basel, Switzerland. This article is an open access article distributed under the terms and conditions of the Creative Commons Attribution (CC BY) license (<https://creativecommons.org/licenses/by/4.0/>).

1. Introduction

Arsenic pollution poses a serious threat to the health of humans and ecosystems [1]. For the human body, this threat is hidden because it may accumulate in plants to a concentration that is harmful to humans, while the plants themselves do not show any signs of phytotoxicity [2]. In the mining industry, arsenic pollution is usually associated with gold and copper mining and processing [3,4]. Arsenopyrite or other arsenic-bearing sulfide minerals in the ore can cause soil pollution, and the contaminated soil can sustainably cause secondary arsenic pollution in the water body, which is easy to spread the pollution to a wider range during the flow process [5]. Once the soil is polluted by arsenic, it is very difficult to control, and the treatment period is long [6,7]. It takes more than 100 years to remove arsenic pollutants in the soil by plant absorption. In order to solve this problem, scholars at home and abroad have proposed adsorption, solidification, and other treatment

technologies, which have partially solved the problem of arsenic solidification, but the high cost of treatment has discouraged the industry. Researchers have turned to the development and optimization of arsenic pollution interception and control materials, limiting the transmission of arsenic pollutants, and controlling arsenic pollution in a limited range at the lowest cost [8].

Arsenic pollutants in water mainly exist in ionic and colloidal states [9]. In order to intercept arsenic pollutants in water, coagulation/flocculation, precipitation, adsorption, ion exchange, membrane filtration, bioremediation, electrochemical treatment, and other technical means have been widely studied for decades [10–12]. These technologies have shown advantages in different aspects in the laboratory, but adsorption is still the most promising treatment method in terms of technical simplicity and cost-effectiveness [13]. Das et al. [14] compared four different adsorbents and verified the effectiveness of nano-magnetite and nano-zero-valent iron on arsenic pollution. It was found that graphene oxide-nano zero-valent iron nanohybrid is the most effective component for removing arsenic pollution in water [15]. Aluminum oxide is also an effective arsenic adsorbent. Amorphous aluminum oxide also has a higher adsorption capacity than crystalline aluminum oxide. The adsorption rate of aluminum oxide to As(V) is the highest in the range of pH = 4–6 [16].

In contrast, the cost of using mineral materials as adsorbents for arsenic pollutants is lower. Among them, natural laterite can reduce the concentration of arsenic in water by about 10 µg/L [17]. Ordinary Portland cement can also be used to solidify and stabilize arsenic pollutants, but cement is obviously not suitable as an interception material for pollutants in water. Although many studies have developed new environmentally friendly materials to replace ordinary Portland cement [18–20], the current research can only explain that alkali-activated materials can be used to stabilize and solidify potentially contaminated soil [21–23]. Fly ash and finely ground blast furnace slag can replace some cement in geotechnical engineering [24], but there is no report on the successful application of similar alternative environmentally friendly materials to arsenic pollutant interception materials. Clay is a fine-grained natural raw material, which has long been widely used as an adsorbent for trace heavy metal ions [25]. The solidification ability of clay minerals to arsenic is lower than that of heavy metals and organic matter, and the adsorption capacity of As (V) is higher than that of As (III). Clay minerals are abundant in reserves, low in cost, good in availability, high in specific surface area, good in adsorption, nontoxic, and have great potential in ion exchange. Compared with other adsorbents, they have many comparative advantages. Ionic arsenic can also be adsorbed by pyrite. It was found that the adsorption rate of arsenic by pyrite was close to 100%, and there was a very fast adsorption rate and low desorption rate [26]. Other natural and synthetic mineral materials, such as activated carbon, activated alumina, zeolite, carbon nanotubes, metal organic frameworks, graphene oxide, zero-valent iron, etc., have also been applied to the study of arsenic removal by adsorption [27]. Some industrial by-products, such as steel slag and fly ash, are also used as low-cost adsorption materials [28,29].

This study proposes the synergistic utilization of steel slag (SS) and desulfurization gypsum (DG), two underutilized industrial solid wastes, as permeable reactive materials for the remediation of arsenic (As) and antimony (Sb)-contaminated water. We systematically investigated key parameters, including particle size optimization of SS and DG, their mass ratio, residence reaction time, and the synergistic mechanism of arsenic stabilization. This study is the first to integrate SS and DG into a permeable reactive barrier system, addressing both the technological gap of low-cost arsenic interception materials and the practical challenges of industrial waste stockpiles. This study not only advances the design of eco-friendly permeable reactive barrier systems but also conforms to the principles of circular economy and provides a scalable solution for mining and industrial areas.

2. Experiment

2.1. Raw Materials

Collection of soil from an arsenic-contaminated area in Yunnan was carried out. In total, 100 kg of contaminated soil was mixed with 25 kg of tap water and soaked, left for 24 h, and the supernatant was taken as the polluted water for the test.

The steel slag (SS) used in the test was obtained from a drum of steel slag provided by Baowu Huanke Wuhan Metal Resources Co., Ltd. in Wuhan, Hubei Province, China. The steel slag was broken and sieved into the following four particle sizes: $+9.5$, $-9.5 + 4.75$, $-4.75 + 1.18$, and -1.18 mm.

The desulfurization gypsum (DG) used in the test was provided by a company in Handan, Hebei Province. In order to investigate the effect of the particle size of desulfurization gypsum on the filtration of polluted water by steel slag-desulfurization gypsum permeable reactive materials, desulfurization gypsum needs to be made into particles with different particle sizes. It was put into a drying box, with the temperature set to $50\text{ }^{\circ}\text{C}$ for 24 h. The dried desulfurization gypsum was placed in an angle grinder for continuous grinding for 1 h. Afterward, 800 g of powdered desulfurization gypsum was transferred into a mixer, where 17% water was added. The mixture was stirred for 5 min and then placed into a self-sealing bag to form into a solid piece. The desulfurization gypsum block was put into the roller press ball machine and pressed into a flat ball with a diameter of 2 cm. The desulfurization gypsum ball was placed in the oven set to $55\text{ }^{\circ}\text{C}$, and the drying time was 24 h. A hammer was used to crush the desulfurization gypsum ball into particles of different sizes, and four particle sizes of $+13.2$, $-13.2 + 9.5$, $-9.5 + 4.75$, and -4.75 mm were screened.

2.2. Experimental Methods

2.2.1. Experimental Materials

In the surface runoff of the contaminated area, the As and Sb contents were 75 and 85 $\mu\text{g/L}$, respectively, and the Cd content was 42 $\mu\text{g/L}$, far exceeding the Class III of GB/T 14,848 (hereinafter referred to as “standard”). The Cr content was within the standard of drinking water (50 $\mu\text{g/L}$), while the Pb, Zn, and Cu contents were slightly higher than the standard of drinking water. To maintain the contaminated water concentration, the experiment was carried out by using tap water to leach contaminated soil and obtain leachate (i.e., leachate of contaminated soil [TLY]) instead of contaminated surface runoff (i.e., actual surface runoff [WRJL]). The composition pairs of harmful elements in WRJL, TLY, and standard are shown in Table 1.

Table 1. Composition of contaminated surface runoff and leachate from contaminated soil (unit: $\mu\text{g/L}$).

Elements	As	Sb	Cr	Pb	Cd	Cu	Hg	Zn
WRJL	75	85	7.4	12	42	1580	<0.01	1070
TLY	81	86	7.1	15	51	1360	<0.01	1550
Standard	10	/	50	10	5	1000	1	1000

Table 1 reveals that the contents of harmful elements, namely, As, Sb, Cd, Pb, and Zn, were slightly higher in TLY than in WRJL, and the contents of Cr and Cu were slightly lower in WRJL. The content of heavy metal elements was less than $0.01\text{ }\mu\text{g/L}$. As the overall element composition was roughly consistent with that of the contaminated soil collected on-site, the contaminated leachate could thus be used to replace the contaminated surface runoff.

2.2.2. Physicochemical Properties of Experimental Materials

The mass fractions of the major elements in the two materials were analyzed using X-ray fluorescence spectrometry (XRF). The chemical compositions of SS and DG are shown in Table 2. The physical phase compositions of SS and DG are shown in Figure 1a,b. In addition, the surface morphology of some composites was examined using BPMA, as shown in Figures 2 and 3.

Table 2. Chemical composition of steel slag and desulfurization gypsum (unit: %).

Elements	Ca	Fe	Mg	Mn	Si	Al	As
Steel slag (SS)	30.35	18.96	4.08	2.14	6.83	1.58	0
Desulfurization gypsum (DG)	21.8	0.251	0	0	0.876	0.328	0
Elements	Cd	Cr	Cu	Hg	Pb	Sb	Zn
Steel slag (SS)	0	0.123	0.001	0	0	0	0.012
Desulfurization gypsum (DG)	0	0.001	0	0	0	0	0.003

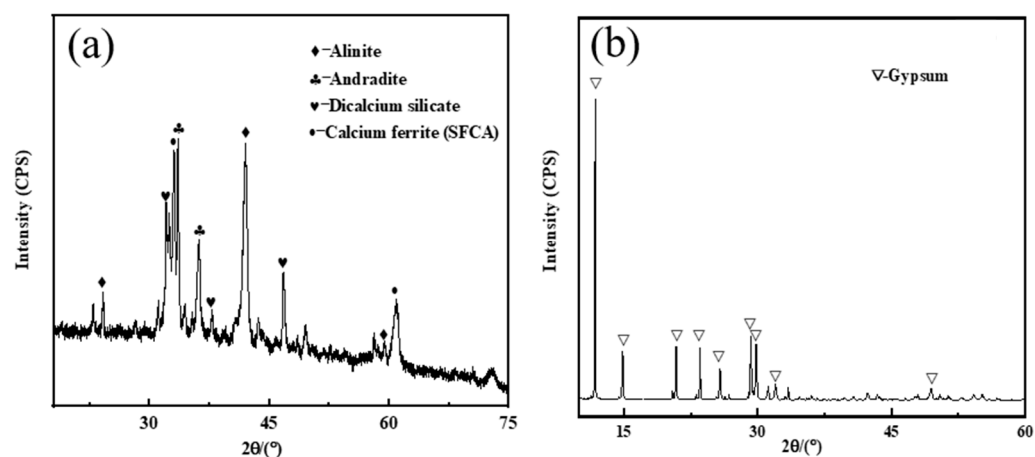


Figure 1. XRD diagram of (a) steel slag and (b) desulfurization gypsum.

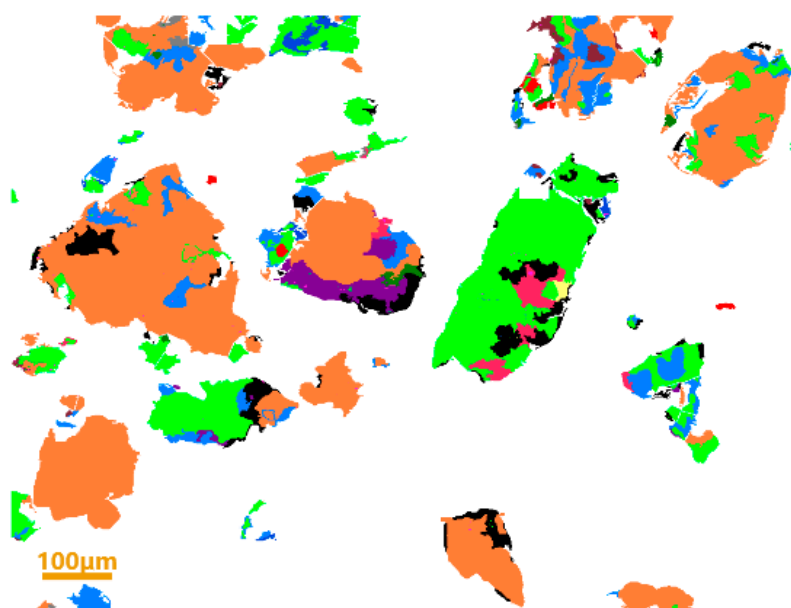


Figure 2. Cont.













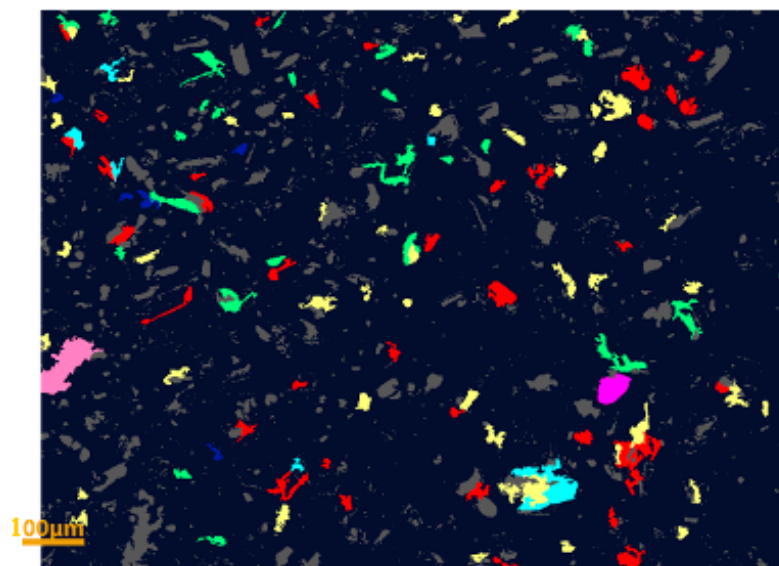
Color						
Mineral	Magnesium ferrite	Calcium ferrite	Calcium silicate	Quartz	Apatite	Fluorite
Content/%	38.5	34.44	13.91	3.94	2.77	1.41
Color						
Mineral	Calcium iron pyroxene	Yellow feldspar	Ferromanganese garnet	Elemental iron	Other	Total
Content/%	1.05	0.96	0.86	0.36	1.8	100.0

Figure 2. BPMA mineral diagram of steel slag.










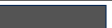
Color				
Mineral	Gypsum	Quartz	Ordinary pyroxene	Dicalcium silicate
Content/%	93.18	2.15	2.84	0.37
Color				
Mineral	Calcite	Calcium ferrite	Dolomite	Other
Content/%	0.21	0.17	0.37	0.71

Figure 3. BPMA mineral diagram of desulfurization gypsum.

Table 2 indicates that the steel slag mainly contains calcium (30.35%), iron (18.96%), silicon (6.83%), and magnesium (4.08%), with other elements making up the remaining percentage. Figures 1a and 2 combined show that the main materials of steel slag are magnesium ferrite, calcium ferrite, and calcium silicate, which have different degrees of encapsulation among one another. The quartz content is 3.94%, which is embedded in the edge or interior of magnesium ferrite and calcium ferrite, and the contents of other minerals, such as apatite, fluorite, and calcium iron pyroxene, are less.

The main elements in desulfurization gypsum are calcium, silicon, aluminum, iron, and other small trace elements. Figures 1b and 3 combined show that the main mineral in desulfurization gypsum is dihydrate gypsum (93.18%), followed by ordinary pyroxene (2.84%) and quartz (2.15%).

2.2.3. Permeable Reactive Barrier Simulation Experiments

The steel slag and desulfurization gypsum of different particle sizes were mixed proportionally and placed in a 1000 mL beaker with the height of the material fixed at 10 cm. Then, 400 mL of polluted water was taken and poured into the beaker. After a certain period of standing time, it was poured out and filtered to obtain the treated contaminated water, and the arsenic and antimony content was measured. The experimental mixing

proportions of permeable reactive materials were as shown in Table 3. Series A, B, and C were designed to control the particle sizes of SS (+9.5, −9.5 + 4.75, −4.75 + 1.18, and −1.18 mm), DG (+13.2, −13.2 + 9.5, −9.5 + 4.75, and −4.75 mm), and the ratios of SS to DG in SS-DG composites (4:1, 2:1, 1:1, and 1:2), respectively. Series D shows the effect of the particle size of the specimen after SS-DG mixing on the filtration of polluted water. Specifically, −0.074 mm steel slag and desulfurization gypsum were mixed in the ratio of 4:1, and then 15% water was added and stirred well. The uniformly mixed specimens (about 12 g at a time) were put into the press mold, and the pressure of the air compressor was set at 20 kN. The mixed specimens were broken into different-sized particles with a hammer and screened into the following three fractions: 13.2 mm, +9.5 mm, −9.5 + 4.75 mm, and −4.75 mm. Series E was simulated by controlling the different residence times of the polluted water through the thickness reaction wall with residence times set to 20, 60, 100, 200, 400, and 800 s. For each series, six sets of parallel experiments were conducted, and the average value was calculated as the final result.

The concentrations of arsenic and antimony in the water were determined by Inductively Coupled Plasma Mass Spectrometry (ICP-MS, Optima 8300, PerkinElmer, USA) and the corresponding removal rate were calculated. The removal rate was calculated according to Equation (1). Desulfurization gypsum and steel slag particles of different sizes are shown in Figures 4 and 5.

$$R = \frac{(C_0 - C_t)}{C_0} \times 100\% \quad (1)$$

where C_0 and C_t are the initial concentration of heavy metal ions and the concentration after permeation reaction ($\mu\text{g/L}$), respectively.



Figure 4. Desulfurization gypsum particles of each particle size.



Figure 5. Steel slag particles of different sizes.

Table 3. Mixing proportions of permeable reactive materials.

No.	Parameters	The Particle Size of SS/mm	The Particle Size of DG/mm	SS: DG	The Particle Size of SS-DG Materials/mm	Residence Time/s
A	The particle size of SS	+9.5, −9.5 + 4.75, −4.75 + 1.18, and −1.18	Unbroken	1:1	—	20
B	The particle size of DG	−4.75 + 1.18	+13.2, −13.2 + 9.5, −9.5 + 4.75, −4.75	1:1	—	20
C	SS: DG	−4.75 + 1.18	−13.2 + 9.5	4:1, 2:1, 1:1, 1:2	—	20
D	The particle size of SS-DG materials	−0.074	−0.074	4:1	13.2, +9.5, −9.5 + 4.74, −4.75	20
F	Residence time	−4.75 + 1.18	−13.2 + 9.5	4:1	—	20, 60, 100, 200, 400, 800

3. Results and Discussion

3.1. Effects of Steel Slag Particle Size on the Removal of Arsenic and Antimony

Figure 6 reveals that the concentration of As in polluted water decreases with the decrease in steel slag particle size, that is, the smaller the steel slag particle size, the better the removal effect of As. The concentration of Sb in polluted water decreases first and then increases with the decrease in steel slag particle size, with the removal rate of Sb increasing first and then decreasing with the decrease in steel slag particle size. The steel slag of −4.75 + 1.18 mm has the best removal effect on Sb. On the whole, when the particle size of steel slag is −4.75 + 1.18 mm, the removal effect of Sb is the best, and the removal rate can reach 56.98%. At this time, the removal rate of As reaches 76.54%, which is a good removal performance. This is due to the fact that when the particle size of steel slag decreases, the SS-DG composite material has a larger specific surface area and adsorption sites and

therefore exhibits adsorption of more As [30]. However, when the particle size of steel slag is less than 1.18 mm, the pore size of the composite material becomes smaller, which may weaken the adsorption capacity of Sb [31].

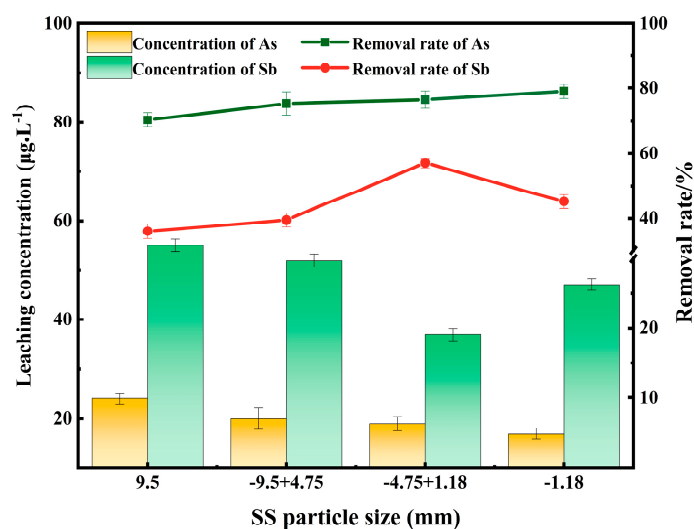


Figure 6. Effects of steel slag particle size on the removal of arsenic and stibium in polluted water.

3.2. Effects of Particle Size of Desulfurized Gypsum on the Removal of Arsenic and Antimony

Figure 7 shows that with the decrease in particle size of desulfurization gypsum, the content of As in polluted water decreases first and then increases, and the removal of As increases first and then decreases. The desulfurization gypsum of $-9.5 + 4.75$ mm has the best removal effect on As. Figure 7 reveals that with the decrease in particle size of desulfurized gypsum, the content of Sb in the polluted water decreases first and then remains basically unchanged [32]. When the particle size of the desulfurized gypsum is $-13.2 + 9.5$ mm, the removal effect of Sb begins to appear. Considering that the crushing processing cost of $-13.2 + 9.5$ mm desulfurized gypsum is lower than that of $-9.5 + 4.75$ mm desulfurized gypsum and it achieves an As removal rate of 81.85% while being less prone to muddying, $-13.2 + 9.5$ mm desulfurized gypsum is preferred.

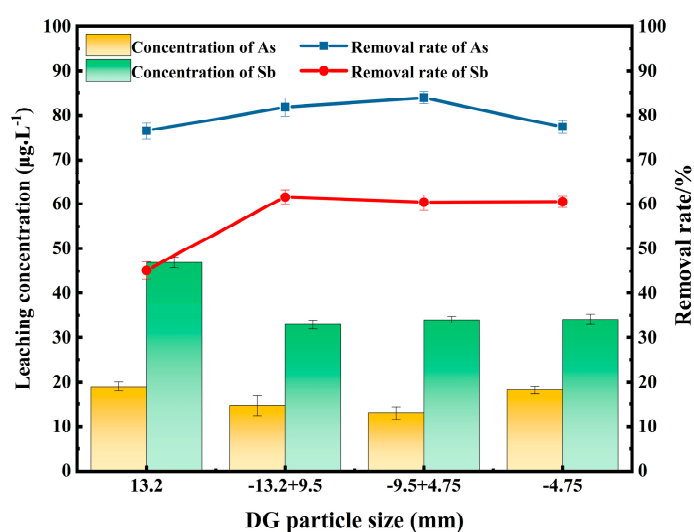


Figure 7. Effects of particle size of desulfurized gypsum on the removal of arsenic and stibium in polluted water.

3.3. Effects of the Ratio of Steel Slag and Desulfurization Gypsum on the Removal of Arsenic and Antimony

Figure 8 shows that the smaller the mass ratio of steel slag to desulfurized gypsum, the greater the As content in the polluted water, indicating that the removal effect of As also worsens. When the ratio of steel slag to desulfurized gypsum is 4:1, the content of As in polluted water is $9.1 \mu\text{g/L}$, which is lower than the standard of drinking water. Similarly, Figure 8 indicates that with the decrease in the mass ratio of steel slag to desulfurized gypsum, the Sb content in the polluted water after treatment gradually increases, and the removal rate of Sb also decreases.

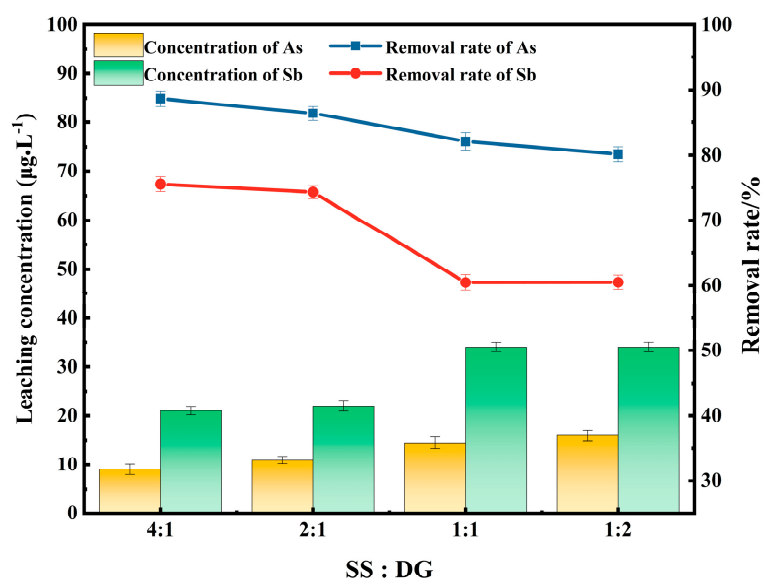


Figure 8. Effects of the ratio of steel slag to desulfurized gypsum on the removal of arsenic and stibium in polluted water.

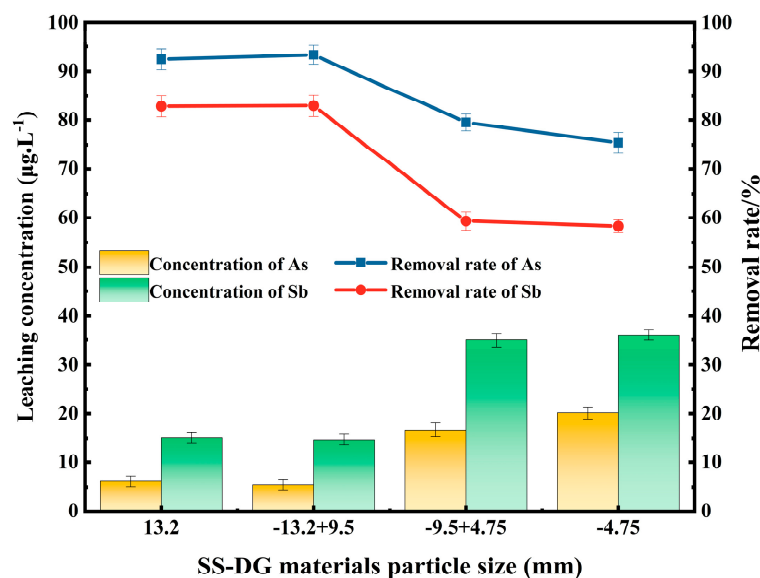
3.4. Effects of Particle Size of SS-DG Mixed Test Block on the Removal of Arsenic and Antimony

During the test, a large number of small bubbles emerged on the unbroken SS-DG mixed test block, indicating that the mixed test block has a porous structure. The mixed test blocks of +9.5, $-9.5 + 4.75$, and -4.75 mm were pulverized during the test, and obvious colloids were formed in the solution. The particle volume was significantly reduced, where the smaller the particle size of the test block, the more serious the pulverization phenomenon. The unbroken and +9.5 mm SS-DG mixed test block has a good effect on the removal of As and Sb, while the +9.5 mm mixed test block has the best removal effect on As and Sb. At this time, the removal rate of As is 93.33%, and the removal rate of Sb is 82.91% (Figure 9).

Table 4 shows the comparison of the removal effect of heavy metals by direct mixing of steel slag and desulfurization gypsum and making mixed test blocks. It reveals that although the SS-DG mixed test block as a filter material has a better removal effect on heavy metals than direct mixing, the As content after treatment is lower than the drinking water standard, while the Sb content is higher than the drinking water standard. Given the high production cost of the SS-DG mixed test block and the ease of pulverizing with the increase in use time, direct mixed steel slag and desulfurization gypsum are still used as filter materials.

Table 4. Comparison of the removal effect of heavy metals by direct mixing of steel slag and desulfurization gypsum and making mixed test blocks.

Filter Material Composition		As Content ($\mu\text{g/L}$)	As Removal Rate (%)	Sb Content ($\mu\text{g/L}$)	Sb Removal Rate (%)
+4.75 mm – 1.18 mm steel slag, –13.2 mm + 9.5 mm desulfurization gypsum mixed with 4:1.		9.1	88.77	21	75.58
Mixed test block	Unbroken	6.1	92.47	15	82.56
	+9.5 mm	5.4	93.33	14.7	82.91

**Figure 9.** Effects of particle size of SS-DG mixed test block on the removal of arsenic and stibium in polluted water.

3.5. Permeable Reactive Wall Thickness Simulation Test

The steel slag with a particle size of $-4.75 + 1.18$ mm and the desulfurization gypsum block with a particle size of $-13.2 + 9.5$ mm were mixed uniformly at a ratio of 4:1 and then loaded into six 1000 mL beakers to a height of 10 cm. Assuming that the flow rate of surface runoff is 0.1 m/s, 400 mL of polluted water was taken and poured out after being left to stand in the beakers for 20, 60, 100, 200, 400, and 800 s, respectively. The thicknesses of the permeable reactive wall were simulated to be 2, 6, 10, 20, 40, and 80 m, respectively [33]. After filtration, the contents of arsenic and antimony were measured.

With the increase in the thickness of the permeable reactive wall, the contents of As and Sb in the treated polluted water gradually decrease, and the decreasing trend gradually slows down (Figure 10). When the thickness of the permeable reactive wall is 40 m, that is, the polluted water stays in the beaker for 400 s, the content of As in the treated polluted water is 6 $\mu\text{g/L}$, and the content of Sb is 3.9 $\mu\text{g/L}$, which is lower than the standard of drinking water. The removal rate of As is 91.85%, and the removal rate of Sb is 90.58%.

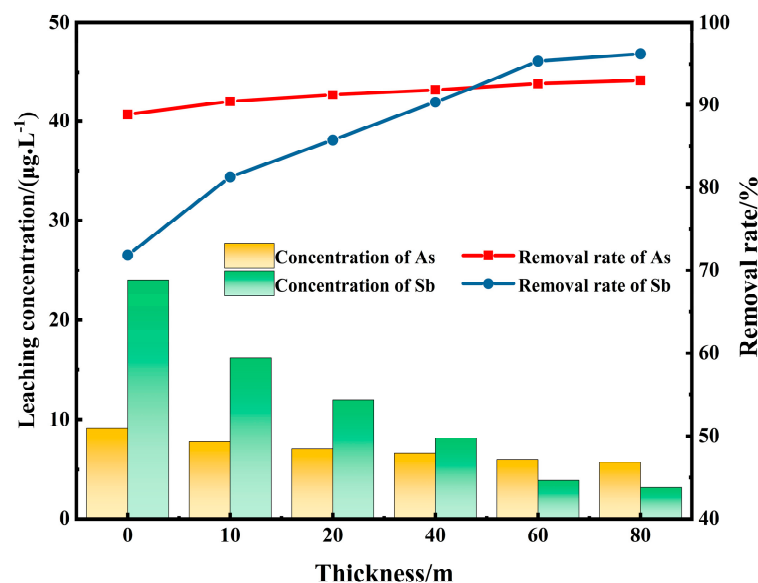


Figure 10. Effects of the thickness of permeable reactive barrier on the removal efficiency of arsenic and stibium.

3.6. EDS Analysis of Arsenic Enrichment Area

Figure 11 shows the microscopic morphology of the medium after treatment of contaminated water with the permeation reactive material made from steel slag and desulfurization gypsum. According to the results of Table 5 EDX elemental composition, it can be seen that the main hydration products of the permeable reactive composites are C-S-H gel and Ettringite. It is suggested that As is mainly solidified by the C-S-H gel formed by the hydration of steel slag and desulfurization gypsum. The C-S-H gel has a large specific surface area and pore space, which can adsorb and physically encapsulate arsenic ions and their compounds [34]. The interception mechanism of arsenic and associated pollutants using all-solid waste interception materials is shown in chemical Equations (2)–(5) [35].



Figure 11. The C-S-H gel and Ettringite minerals formed in the interception materials layer.

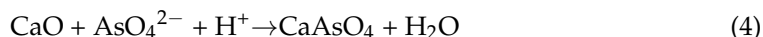
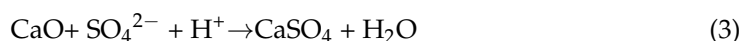
Table 5. EDX element composition of the compounds in SEM images (wt.%).

	Compounds	Ca	O	Al	Si	S	Fe	As
Point 1	Ettringite	63.31	8.51	4.89	5.99	16.02	0.81	0.47
Point 2	C-S-H gel	17.89	43.36	2.42	29.25	0.61		6.47

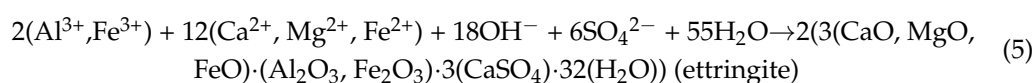
Arsenic leaching mechanism (in pollution site):



Arsenic stabilization mechanism (in the intercepting material layer):



Arsenic curing mechanism (in the intercepting material layer): typical steel slag contains a large amount of divalent metal oxide components ($\text{CaO} + \text{MgO} + \text{FeO}$) [36], and the total content can reach more than 70%. These components can stimulate the sediment colloids intercepted by the interception wall to form C-S-H gel and can also capture Al_2O_3 and Fe_2O_3 in the steel slag silicate minerals with the participation of CaSO_4 to form ettringite and other double salt minerals (shown in Equation (5) and Figure 11). Arsenic-containing contaminants stabilized as CaAsO_4 minerals are further solidified in C-S-H gel and Ettringite minerals [37].



The ionic and colloidal arsenic elements in the water were intercepted by the interception material layer (Figure 12). Among them, the ionic arsenic element was stabilized as CaAsO_4 mineral to lose migration activity and is wrapped and solidified with colloidal arsenic element in the newly formed C-S-H gel and ettringite mineral, thereby eliminating arsenic pollution in the water body [38].

Arsenic contamination process

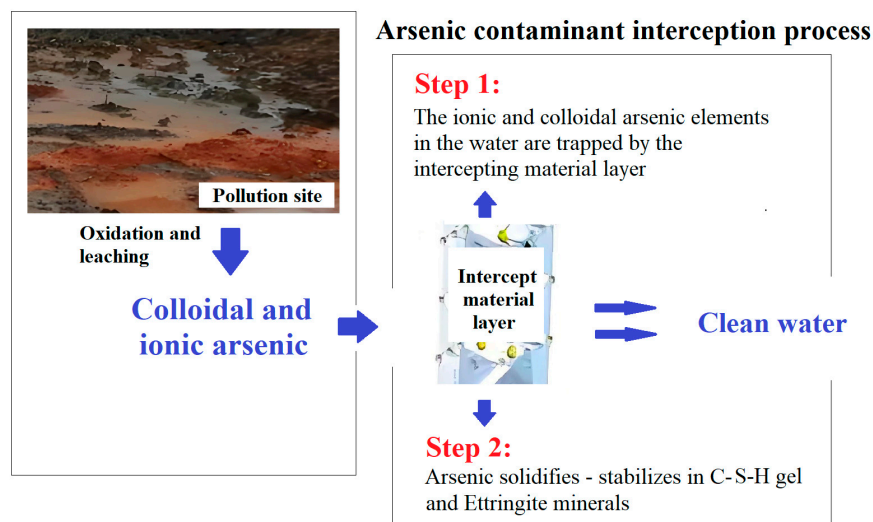


Figure 12. The process of intercepting arsenic pollutants.

4. Conclusions

- (1) The effects of the particle sizes of steel slag and desulfurization gypsum, the ratio of steel slag to desulfurization gypsum, and the particle size of the SS-DG mixed test block on the removal of arsenic and antimony by the permeable reactive wall were investigated. Results indicated that the steel slag with a particle size of $-4.75 + 1.18$ mm and the desulfurization gypsum block with a particle size of $-13.2 + 9.5$ mm mixed evenly at a ratio of 4:1 make a 40 m permeable reactive wall. After treatment, the As content in the polluted water was $6 \mu\text{g/L}$, and the Sb content was $3.9 \mu\text{g/L}$, which was lower than the standard of drinking water. The removal rates of As and Sb were 91.85% and 90.58%, respectively. The purpose of using steel slag and desulfurization gypsum to intercept heavy metals and toxic ions in surface runoff was achieved.

- (2) The formation of C-S-H gel and ettringite in the dielectric material is the main way to stabilize As. This stabilization occurs through several processes, including the adsorption, physical encapsulation, and lattice solidification of C-S-H gel, as well as the ion exchange reaction of ettringite with arsenic ions and arsenate. Together, these mechanisms can synergistically improve the stabilization effect of As.
- (3) Although this study confirmed the efficient removal of arsenic and antimony by SS-DG composites, the following limitations and research gaps still exist: the experiments were based on laboratory simulation conditions without considering the effects of the dynamic flow of groundwater and the interfering effects of competing ions in practical applications; the long-term stability of the materials and the adsorption mechanism still need to be verified; in addition, the engineering feasibility of large-scale applications and the assessment of the environmental benefits of the whole life cycle. In addition, the engineering feasibility of large-scale application and the assessment of the environmental benefits of the whole life cycle have not been carried out. In the future, it is necessary to combine dynamic flow field experiments and field pilot tests to improve the practicality and sustainability of the technology.

Author Contributions: Conceptualization, Y.L. and W.N.; methodology, Y.L. and Y.S.; software, D.W. (Dongxu Wu); validation, S.Y., D.W. (Dongfang Wang) and W.H.; formal analysis, Y.L. and W.H.; investigation, D.W. (Dongfang Wang); resources, W.H.; data curation, Y.S.; writing—original draft preparation, Y.S. and Y.L.; writing—review and editing, Y.L.; visualization, W.H. and D.W. (Dongfang Wang); supervision, W.H.; project administration, W.H.; funding acquisition, W.N. and W.H. All authors have read and agreed to the published version of the manuscript.

Funding: This study was supported by the National Key Research and Development Program of China (No. 2020YFC1807803).

Data Availability Statement: The raw data supporting the conclusions of this article will be made available by the authors on request.

Conflicts of Interest: The authors declare no conflicts of interest.

References

- Sultan, M.W.; Qureshi, F.; Ahmed, S.; Kamyab, H.; Rajendran, S.; Ibrahim, H.; Yusuf, M. A comprehensive review on arsenic contamination in groundwater: Sources, detection, mitigation strategies and cost analysis. *Environ. Res.* **2025**, *265*, 120457. [[CrossRef](#)] [[PubMed](#)]
- Yang, Y.; Chen, W.; Meng, D.; Ma, C.; Li, H. Investigation of arsenic contamination in soil and plants along the river of Xinzhou abandoned gold mine in Qingyuan, China. *Chemosphere* **2024**, *359*, 142350. [[CrossRef](#)] [[PubMed](#)]
- Strawn, D.G. Review of interactions between phosphorus and arsenic in soils from four case studies. *Geochem. Trans.* **2028**, *19*, 10. [[CrossRef](#)]
- Jin, Y.; Zhu, W.; Li, J.; Cui, D.; Zhang, Z.; Sun, G.; Zhu, Y.; Yang, H.; Zhang, X. Arsenic pollution concerning surface water and sediment of Jie River: A pilot area where gold smelting enterprises are concentrated. *Environ. Res.* **2024**, *249*, 118384. [[CrossRef](#)]
- Tian, S.; Liu, Z.; Mao, Q.; Ye, H.; Tian, C.; Zhu, Y.; Zhang, L. Leaching characteristics and environmental impact of heavy metals in tailings under rainfall conditions: A case study of an ion-adsorption rare earth mining area. *Ecotoxicol. Environ. Saf.* **2024**, *281*, 116642. [[CrossRef](#)]
- Rinklebe, J.; Antoniadis, V.; Shaheen, S.M.; Rosche, O.; Altermann, M. Health risk assessment of potentially toxic elements in soils along the Central Elbe River, Germany. *Environ. Int.* **2019**, *126*, 76–88. [[CrossRef](#)]
- Sevak, P.; Pushkar, B. Arsenic pollution cycle, toxicity and sustainable remediation technologies: A comprehensive review and bibliometric analysis. *J. Environ. Manag.* **2024**, *349*, 119504. [[CrossRef](#)]
- Choudhury, T.R.; Alam, S.; Alam, M.N.E.; Maksud, M.A.; Khan, S.R.; Habib, M.A. Innovative metal–phenolic nanocomposite sorbent: A groundbreaking solution for arsenic-free drinking water—Synthesis and characterization approaches. *Desalin. Water Treat.* **2024**, *320*, 100764. [[CrossRef](#)]
- Bauer, M.; Blodau, C. Arsenic distribution in the dissolved, colloidal and particulate size fraction of experimental solutions rich in dissolved organic matter and ferric iron. *Geochim. Cosmochim. Acta* **2009**, *73*, 529–542. [[CrossRef](#)]

10. Ghosh, S.; Debsarkar, A.; Dutta, A. Technology alternatives for decontamination of arsenic-rich groundwater—A critical review. *Environ. Technol. Innov.* **2019**, *13*, 277–303. [[CrossRef](#)]
11. Kobya, M.; Soltani, R.D.C.; Omwene, P.I.; Khataee, A. A review on decontamination of arsenic-contained water by electrocoagulation: Reactor configurations and operating cost along with removal mechanisms. *Environ. Technol. Innov.* **2020**, *17*, 100519. [[CrossRef](#)]
12. Bahar, M.M.; Mahbub, K.R.; Naidu, R.; Megharaj, M. As(V) removal from aqueous solution using a low-cost adsorbent coir pith ash: Equilibrium and kinetic study. *Environ. Technol. Innov.* **2018**, *9*, 198–209. [[CrossRef](#)]
13. Yadav, M.K.; Saidulu, D.; Ghosal, P.S.; Mukherjee, A.; Gupta, A.K. A review on the management of arsenic-laden spent adsorbent: Insights of global practices, process criticality, and sustainable solutions. *Environ. Technol. Innov.* **2022**, *27*, 102500. [[CrossRef](#)]
14. Das, T.K.; Bezbaruah, A.N. Comparative study of arsenic removal by iron-based nanomaterials: Potential candidates for field applications. *Sci. Total Environ.* **2021**, *764*, 142914. [[CrossRef](#)]
15. Wang, S.; Mulligan, C.N. Natural attenuation processes for remediation of arsenic contaminated soils and groundwater. *J. Hazard. Mater.* **2006**, *138*, 459–470. [[CrossRef](#)]
16. Álvarez-Ayuso, E.; Murciego, A. Stabilization methods for the treatment of weathered arsenopyrite mine wastes: Arsenic immobilization under selective leaching conditions. *J. Clean. Prod.* **2021**, *283*, 125265. [[CrossRef](#)]
17. Nguyen, T.H.; Tran, H.N.; Vu, H.A.; Trinh, M.V.; Nguyen, T.V.; Loganathan, P.; Vigneswaran, S.; Nguyen, T.M.; Trinh, V.T.; Vu, D.L.; et al. Laterite as a low-cost adsorbent in a sustainable decentralized filtration system to remove arsenic from groundwater in Vietnam. *Sci. Total Environ.* **2020**, *699*, 134267. [[CrossRef](#)]
18. Liu, Y.; Ni, J.; Gu, J.; Liu, S.; Huang, Y.; Sadeghi, H. Influence of biopolymer-vegetation interaction on soil hydro-mechanical properties under climate change: A review. *Sci. Total Environ.* **2024**, *954*, 176535. [[CrossRef](#)]
19. Ghadir, P.; Zamanian, M.; Mahbubi-Motlagh, N.; Saberian, M.; Li, J.; Ranjbar, N. Shear strength and life cycle assessment of volcanic ash-based geopolymer and cement stabilized soil: A comparative study. *Transp. Geotech.* **2021**, *31*, 100639. [[CrossRef](#)]
20. Wang, H.; Ju, C.; Zhou, M.; Chen, J.; Dong, Y.; Hou, H. Sustainable and efficient stabilization/solidification of Pb, Cr, and Cd in lead-zinc tailings by using highly reactive pozzolanic solid waste. *J. Environ. Manag.* **2022**, *306*, 114473. [[CrossRef](#)]
21. Chen, H.; Yuan, H.; Mao, L.; Hashmi, M.Z.; Xu, F.; Tang, X. Stabilization/solidification of chromium-bearing electroplating sludge with alkali-activated slag binders. *Chemosphere* **2020**, *240*, 124885. [[CrossRef](#)] [[PubMed](#)]
22. Khadka, S.D.; Jayawickrama, P.W.; Senadheera, S.; Segvic, B. Stabilization of highly expansive soils containing sulfate using metakaolin and fly ash based geopolymer modified with lime and gypsum. *Transp. Geotech.* **2020**, *23*, 100327. [[CrossRef](#)]
23. Zhou, X.; Zhang, Z.-F.; Yang, H.; Bao, C.-J.; Wang, J.-S.; Sun, Y.-H.; Liu, D.-W.; Shen, P.-L.; Su, C. Red mud-metakaolin based cementitious material for remediation of arsenic pollution: Stabilization mechanism and leaching behavior of arsenic in lollingite. *J. Environ. Manag.* **2021**, *300*, 113715. [[CrossRef](#)] [[PubMed](#)]
24. Lee, W.-H.; Cheng, T.-W.; Ding, Y.-C.; Lin, K.-L.; Tsao, S.-W.; Huang, C.-P. Geopolymer technology for the solidification of simulated ion exchange resins with radionuclides. *J. Environ. Manag.* **2019**, *235*, 19–27. [[CrossRef](#)]
25. Nieder, R.; Benbi, D.K.; Scherer, H.W. Fixation and defixation of ammonium in soils: A review. *Biol. Fertil. Soils* **2011**, *47*, 1–14. [[CrossRef](#)]
26. Osorio-López, C.; Seco-Reigosa, N.; Garrido-Rodríguez, B.; Cutillas-Barreiro, L.; Arias-Estévez, M.; Fernández-Sanjurjo, M.J.; Álvarez-Rodríguez, E.; Núñez-Delgado, A. As(V) adsorption on forest and vineyard soils and pyritic material with or without mussel shell: Kinetics and fractionation. *J. Taiwan Inst. Chem. Eng.* **2014**, *45*, 1007–1014. [[CrossRef](#)]
27. Wang, Y.; Liu, H.; Wang, S.; Li, X.; Wang, X.; Jia, Y. Simultaneous removal and oxidation of arsenic from water by δ -MnO₂ modified activated carbon. *J. Environ. Sci.* **2020**, *94*, 147–160. [[CrossRef](#)]
28. Ayala, J.; Fernández, B. Industrial waste materials as adsorbents for the removal of As and other toxic elements from an abandoned mine spoil heap leachate: A case study in Asturias. *J. Hazard. Mater.* **2020**, *384*, 121446. [[CrossRef](#)]
29. Shaikh, W.A.; Alam, M.A.; Alam, M.O.; Chakraborty, S.; Owens, G.; Bhattacharya, T.; Mondal, N.K. Enhanced aqueous phase arsenic removal by a biochar based iron nanocomposite. *Environ. Technol. Innov.* **2020**, *19*, 100936. [[CrossRef](#)]
30. Nguyen, T.-B.; Ho, T.-B.-C.; Huang, C.P.; Chen, C.-W.; Chen, W.-H.; Hsieh, S.; Hsieh, S.-L.; Dong, C.-D. Adsorption of lead(II) onto PE microplastics as a function of particle size: Influencing factors and adsorption mechanism. *Chemosphere* **2022**, *304*, 135276. [[CrossRef](#)]
31. Vannier, S.; Gossard, A.; Magnier, L.; Proust, V.; David, T.; Grandjean, A. Effects of adding zeolite particles on the hierarchical microstructure of zeolite-geopolymer composites and their Sr²⁺ adsorption properties. *Mater. Des.* **2024**, *244*, 113233. [[CrossRef](#)]
32. Xie, H.; Chen, Y.; Chen, X.; Yan, H. Fulvic acid removal from landfill contaminated groundwater by a permeable reactive barrier: From laboratory to field-scale analyses. *J. Environ. Chem. Eng.* **2024**, *12*, 114752. [[CrossRef](#)]
33. Sakr, M.; El Agamawi, H.; Klammler, H.; Mohamed, M.M. A review on the use of permeable reactive barriers as an effective technique for groundwater remediation. *Groundw. Sustain. Dev.* **2023**, *21*, 100914. [[CrossRef](#)]
34. Zhang, X.; Zhang, X.; Li, X.; Liu, Y.; Yu, H.; Ma, M. Porous geopolymer with controllable interconnected pores—A viable permeable reactive barrier filler for lead pollutant removal. *Chemosphere* **2022**, *307*, 136128. [[CrossRef](#)] [[PubMed](#)]

35. Zhang, J.; Yang, F.; Yao, X.; Cao, H.; Duan, W.; Dong, X. The synergistic action mechanisms of ternary industrial waste stabilized lead ion contaminated soil. *Constr. Build. Mater.* **2023**, *409*, 133827. [[CrossRef](#)]
36. Lawrinenko, M.; Kurwadkar, S.; Wilkin, R.T. Long-term performance evaluation of zero-valent iron amended permeable reactive barriers for groundwater remediation—A mechanistic approach. *Geosci. Front.* **2023**, *14*, 101494. [[CrossRef](#)]
37. Ma, M.; Ha, Z.; Lv, C.; Xu, X.; Li, C.; Du, D.; Zhang, T.C.; Chi, R. A novel passivator based on electrolytic manganese residues and calcite for arsenic sorption and heavy metal passivation of contaminated soil. *J. Clean. Prod.* **2023**, *414*, 137544. [[CrossRef](#)]
38. Mei, Y.; Zhuang, S.; Wang, J. Adsorption of heavy metals by biochar in aqueous solution: A review. *Sci. Total Environ.* **2025**, *968*, 178898. [[CrossRef](#)]

Disclaimer/Publisher's Note: The statements, opinions and data contained in all publications are solely those of the individual author(s) and contributor(s) and not of MDPI and/or the editor(s). MDPI and/or the editor(s) disclaim responsibility for any injury to people or property resulting from any ideas, methods, instructions or products referred to in the content.